Effect of Ta Content on the Microstructure and Properties of Laser Cladding Ni60A/WC Composite Coatings

XU HUANG,[1,2] JINYU YU,[2] JIBIN JIANG,[2,3] GUOFU LIAN,[2] CHANGRONG CHEN,[2] MENGNING ZHOU,[2] WEIQI XU,[2] and XINXIN HU[2]

1.—Fujian Key Laboratory of Intelligent Machining Technology and Equipment, Fujian University of Technology), Fuzhou 350118, China. 2.—Fujian University of Technology, Fuzhou 350118, China. 3.—e-mail: jibinj@fjut.edu.cn

Our aim is to solve the problems of cracking and porosity of laser cladding Ni60A/WC high-hardness composite coatings. Ta powder was added to synthesize TaC in situ with C in a molten pool, to reduce the carbon content of the metal matrix and inhibit the generation of carbon oxide gases to obtain a new Ni60A/WC composite coating with no defects, reasonable hard phase distribution, and excellent properties. The phase composition, microstructure, elemental distribution, and mechanical properties of the composite coating were studied by x-ray diffraction, scanning electron microscopy, and tribometry. The results show that Ta more easily combines with C. Adding an appropriate amount of Ta powder inhibits the formation of other carbides and carbon oxide gases, and significantly reduces the cracking sensitivity of the cladding layer. The fine TaC particles synthesized in situ are used as nucleation sites to significantly refine grains and improve microstructure uniformity. In addition, TaC particles with high hardness and good wear resistance also improve the microhardness and wear resistance of the cladding layer, which can provide a reference for the preparation of nickel-based composite coatings with excellent properties.

INTRODUCTION

Laser cladding is a surface modification technology that uses a high-energy laser beam to melt the cladding material and the substrate surface simultaneously, to form a micromolten pool that is solidified rapidly ($10^4 \sim 10^{11}$ K/s) to obtain a coating with excellent performance.[1] The 45 steel is a medium-carbon high-quality steel widely used in engineering, but, in harsh environments, the surface is severely worn, and its surface usually needs to be strengthened. According to current research, a single-phase coating struggles to meet application requirements. The preparation of metal matrix composite coatings by laser cladding technology can significantly improve the performance of the coating.[2] Among them, nickel-based alloys have

attracted much attention because of their high wear and corrosion resistance.[3] In the ceramic-reinforced phase, WC has the characteristics of a high melting point, high hardness, excellent wear resistance, and good wettability with nickel-based alloys.[4,5] Therefore, WC is widely used in composite coatings to improve the service life of parts. At present, there have been many studies on nickel-based WC composite coatings, but there are still problems, such as cracks and pores,[6] and WC particles in the molten pool decompose when heated under the action of a high-energy laser beam. For nickel-based melts, the substantial decomposition of WC particles usually leads to the precipitation of secondary phases, such as Fe_3W_3C, Ni_2W_4C, $Cr_{23}C_6$, and Mo_3W_3C, which significantly increases the inhomogeneity of the cladding microstructure, and the existence of a complex galvanic couple also aggravates electrochemical corrosion.[7] However, in a high-energy environment, the decomposition of WC can hardly be avoided, and a small amount of W can also

strengthen the solid solution.[8] Regulating the decomposition behavior of WC can optimize the performance of the composite coating. Therefore, using the decomposition behavior of WC to improve the performance of the cladding layer has scientific and potential application value. In addition, due to the rapid heating and cooling processes of laser cladding, the residual stress is relatively large, and there are a large number of hard and brittle primary carbides in the cladding layer at the same time, which makes cracks expand easily along the grain boundaries of these carbides, further increasing the cracking sensitivity of the cladding layer. To solve the above problems, it is feasible to introduce strong carbide elements into cladding materials. Hulka et al.[9] prepared Ti-added WC–Co/NiCrBSi composite coatings by laser cladding technology, and studied the effect of Ti on the microstructure and the corrosion resistance of WC–Co/NiCrBSi composite coatings. TiC was synthesized in situ in the molten pool after adding Ti. Under optimal power, the carbide distribution of the cladding layer was uniform, the cracking sensitivity of the coating was reduced, and the microhardness and corrosion resistance were improved. Liu et al.[10] prepared a Ni60 composite coating with Nb added by laser cladding technology, and studied the effect of the Nb content on the cracking sensitivity of a Ni60 alloy coating. After adding nano-Nb powder, the coarse hard phase was refined, the columnar crystals were transformed into equiaxed crystals, a separated eutectic structure was formed, and the cracking sensitivity of the cladding layer was significantly reduced.

Ta has the advantages of having a high melting point, high strength, and excellent wear resistance, and is widely used in metallurgy, machinery, and other fields. As a strong carbide-forming element, it reacts easily with C in the molten pool to form TaC, which can inhibit grain growth and refine the microstructure of the cladding layer, thereby improving its mechanical properties.[11,12] Hu et al.[13] prepared a NiCuBSi/WC composite coating with Ta added to a 5Cr5MoSiV1 steel substrate by laser cladding technology, and studied the effect of Ta addition on the structure and properties of the coating. The study found that, after adding Ta, TaC was synthesized in situ, which improved the uniformity of the hardness distribution in the cladding layer, while the wear resistance of the cladding layer increased by 2.3 times. Qilin et al.[14] prepared a Ni45 + Ta composite coating on the surface of 45 steel by laser cladding technology. It was found that a TaC hard phase was formed in situ between the Ta and C, and that the growth of the eutectic structure of the coarse primary carbides M_7C_3 and γ-Ni + $M_{23}C_6$ was inhibited, which refined the structure of the coating and reduced its cracking sensitivity. After adding 5% Ta, the microhardness and wear resistance of the cladding layer were increased by 18% and 20%, respectively.

Therefore, this study added different contents of Ta powder into a Ni60A/WC composite powder, based on the inherent attributes of Ta as a strong carbide-forming element that inhibits the growth of coarse primary carbides in the cladding layer, in order to reduce the cracking sensitivity of the cladding layer and reduce the generation of cracks. By analyzing the changes in microstructure, phase, and mechanical properties, the effect of Ta powder addition on the cladding layer was obtained, and the best addition content was found. In addition, through the in situ reaction between Ta and C in the molten pool, a fine and evenly distributed TaC hard phase was generated to improve the hardness and wear resistance of the cladding layer, further optimizing the microstructure and properties of the Ni60A/WC composite coating.

MATERIALS AND EXPERIMENTAL PROCEDURES

Materials

In this experiment, 45 steel was selected as the substrate with dimensions of 40 mm × 20 mm × 10 mm, and its chemical composition is shown in supplementary Table S-1 (refer to online supplementary material). Before laser cladding, the surface of the substrate was polished with sandpaper to remove rust and oxides. Then, the polished substrate surface was wiped with absolute ethanol to remove oil stains, and then air-dried. The cladding materials were Ni60A, WC, and Ta powders (all from Zhangzhou QUARK Metal Products, Zhangzhou, China). Scanning electron microscopy (SEM) images of the three powders are shown in supplementary Fig. S-1, showing that the Ni60A powder is smooth and spherical, the WC powder has angular particles, and the Ta powder is irregularly flocculated. The particle size of the Ni60A powder is 48–106 μm, the particle size of the WC powder is 48–100 μm, the particle size of the Ta powder is 50–100 μm. The chemical composition of Ni60A is shown in supplementary Table S-2. In the cladding material, a ratio of Ni60A to WC at 4:1 was maintained while adding different contents of Ta powder. The specific formula is shown in Table I.

Table I. (Ni60A + WC + Ta) composite cladding powder ratio (wt.%)

Sample number	Ni60A	WC	Ta
S1	80	20	0
S2	78.4	19.6	2
S3	76	19	5
S4	72	18	10
S5	68	17	15
S6	64	16	20

Experimental

Before laser cladding, powders with varying proportions were ball-milled using a planetary ball mill. The ball-milling parameters were a milling speed of 200 rpm, a ball-to-powder weight ratio of 3:1, and the ball-milling time was 1 h. After ball milling, the cladding powder was removed, 5 wt.% of polyvinyl alcohol binder was added, the powder was preplaced on the surface of the substrate under a pressure of 100 MPa, and the thickness of the preplaced coatings was approximately 1 mm. Then, the sample was placed in a vacuum dryer at 80°C for 2 h. Finally, the laser cladding was carried out by using a fiber laser (YLS-3000; IPG, Burbach, Germany), and the equipment structure is shown in supplementary Fig. S-2. According to a literature research and preliminary experiment results, the laser cladding parameters included a laser power of 1600 W, a scanning speed of 5 mm/s, a defocusing distance of 10 mm, and argon shielding gas.

Characterization

The particle size of WC in the cladding layer was measured by the particle size analysis software, Nano Measure. The phase of the cladding layer was identified by an x-ray diffractometer (XRD; Ultima IV; Rigaku, Japan) at a scanning speed of 8°/min in the range of 10°–80°. SEM (TM3030Plus, Hitachi, Japan) and energy dispersive spectrometry (EDS) were used to analyze the microstructure and composition of the coatings. Interface bonding performance A friction and a wear tester (UMT-2; Bruker, Germany) was used to evenly apply a load to the bonding interface until the matrix and the cladding layer were completely separated. The microhardness from the top of the cladding layer to the substrate was measured by a microhardness tester (MVA-402TS; HDNS, Shanghai), and the load and duration used for each hardness measurement were 1000 g and 20 s, respectively. Then, the test was repeated 3 times at similar positions, and the average value was taken. Before the friction and wear testing, the surface of the sample was polished with sandpaper of the same particle size to avoid the influence of surface roughness on the wear resistance of the cladding layer and then cleaned with absolute ethanol. The wear resistance of the coatings was tested using a tribometer (UMT-2; Bruker) under dry friction conditions. A tungsten steel ball with a diameter of 10 mm was used as the friction pair. The wear-testing machine motion mechanism was reciprocating. The stroke distance was 3 mm, the sliding speed was 10 mm/s, the applied load was 25 N, and the sliding time was set at 30 min at room temperature. After the friction and wear testing, the sample was cleaned with absolute ethanol. The three-dimensional morphology of the wear area was observed by a white light interferometer integrated with the UMT-2, and the degree of wear was calculated. The wear amount is calculated by multiplying the cross-sectional area by the friction and wear length.

RESULTS AND DISCUSSION

Macromorphology of Cladding Layer

The macromorphology of the single-layer single-pass cladding layer is shown in Fig. 1, demonstrating that the cladding layer of the S1–5 samples was straight and had good forming quality, while the cladding layer flatness of the S6 sample decreased, the surface fluctuated, and more unmelted particles adhered to both sides of the cladding layer. The number of cracks in the S1–S6 samples first decreased and then increased, among which the number of cracks in S1 was the largest and the most obvious, and the number of cracks in S4 was the least. According to the results of the dye penetration test, for the Ni60A/WC composite coating, adding an appropriate amount of Ta powder can reduce the number of cracks in the cladding layer. However, when excess Ta powder is added, the forming quality of the cladding layer decreases. The stress concentration caused by surface defects increases the number of cracks instead of decreasing them.

Figure 2 shows an SEM image of the cross-section of a single cladding layer, indicating that the WC particles of the six groups of samples were evenly distributed in the cladding layer. According to the research of Xiao et al.,[15] when the mass fraction of WC particles in the cladding layer does not exceed 36%, the particles can be evenly distributed in the cladding layer due to Marangoni flow in the molten pool. The difference in this study is that there were obvious pores in the S1 sample, and a crack ran through the pores, while the pores or cracks in the cross-section of the cladding layer with Ta powder were significantly reduced. For the S1 sample, C in the molten pool will form CO or CO_2 with the surrounding O.[16] Ta combines more easily with C, so the formation of pores is inhibited after the addition of Ta powder. In addition, Fig. 2a shows that the WC particles in the cladding layer of the S1 sample were similar to the original WC powder, with large particle sizes, and that most of them had sharp edges and corners. The sharp corners of the WC particles easily cause stress concentration at the tip of the cladding layer, and increase the cracking sensitivity of the cladding layer.[17,18] When Ta powder was added to the cladding material, the morphology of the WC particles in the cladding layer changed significantly, and the WC particles dissolved at the edges and corners, which inhibited the stress concentration at the tip of the hard phase. It can be seen from the figure that the dilution rate of the S4 sample is relatively low.

Shear strength properties were tested on the S4 samples. When the applied load reaches 128.58 N, the matrix and the cladding layer are forcibly separated. The experimental data show that, with the cladding of the S4 sample, the layer forms a
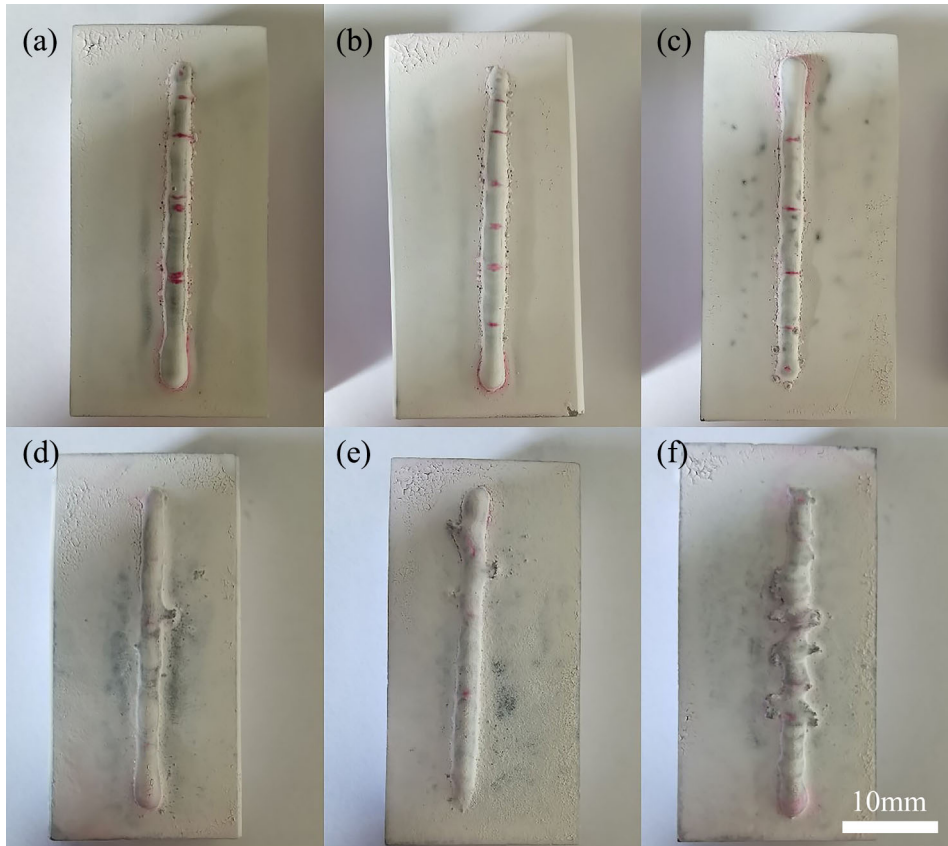
Fig. 1. Macromorphology of the single-layer and single-pass cladding layers: (a) S1, (b) S2, (c) S3, (d) S4, (e) S5, and (f) S6.
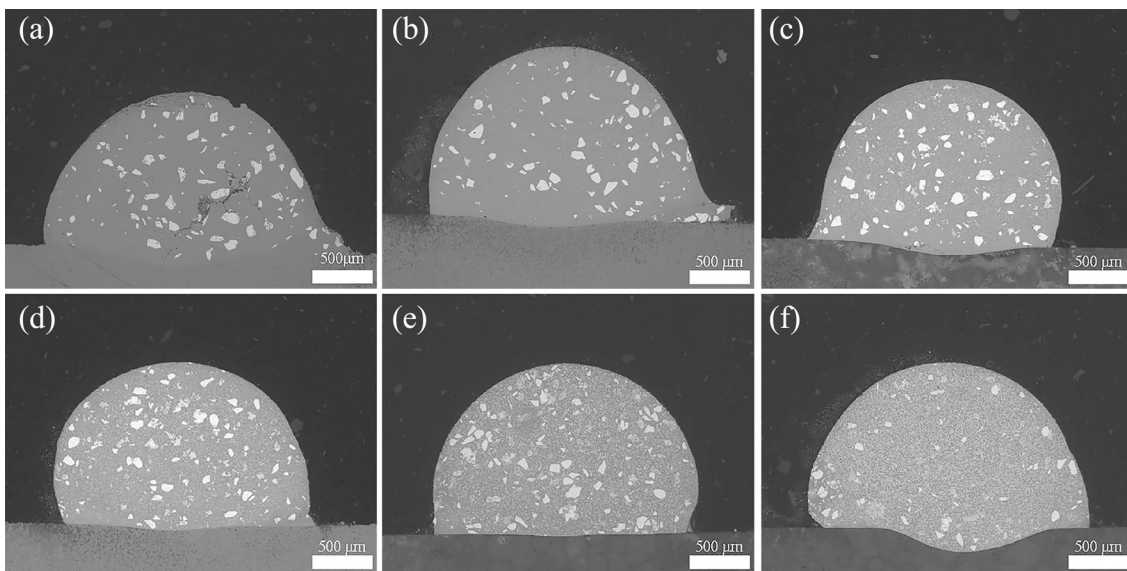

Fig. 2. Cross-sectional morphology of the single-layer and single-pass cladding layers: (a) S1, (b) S2, (c) S3, (d) S4, (e) S5, and (f) S6.

good metallurgical bond with the matrix. Figure 3 shows the frequency diagram and cumulative frequency distribution diagram of WC with different particle sizes in the cladding layer. As shown in Fig. 3a and b, the size of the WC particles decreased with increasing Ta powder content. WC will

decompose into W and C elements in the molten pool under a high-energy laser. The reaction equation is shown in Eqs. 1 and 2. After adding Ta powder, as a strong carbide-forming element, Ta easily reacts with free C in the molten pool to form TaC. The reaction equation is shown in Eq. 3.[19] The
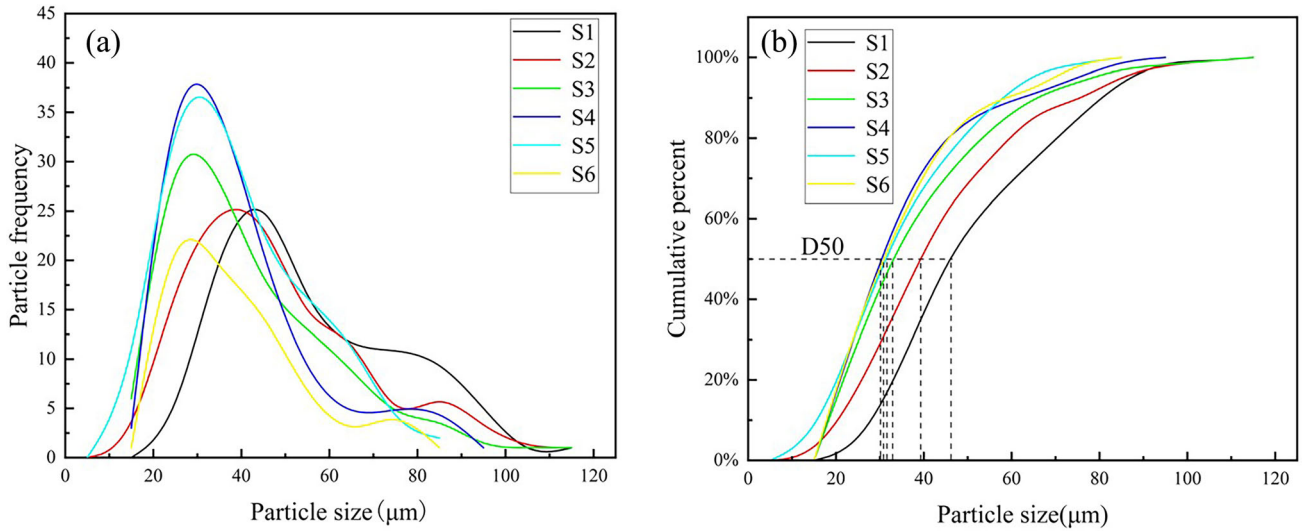
Fig. 3. Frequency diagram and cumulative frequency distribution diagram of the WC particle size in the cladding layer: (a) frequency diagram, and (b) cumulative frequency distribution diagram.

Gibbs free energy of Eq. 3 is less than 0, indicating that the reaction can proceed spontaneously, so the concentration of C in the molten pool will decrease. The decrease of product concentration in Eqs. 1 and 2 will promote the reaction to move toward the product direction, that is, promote the dissolution of the WC particles.

$$2WC = W_2C + C \tag{1}$$

$$W_2C = 2W + C \tag{2}$$

$$Ta(s) + C(s) = TaC(s)\Delta G\frac{\theta}{TaC} = -142.25 + 0.023T \tag{3}$$
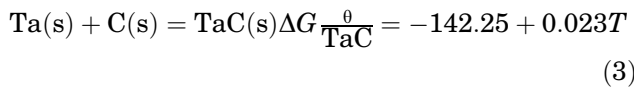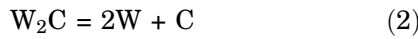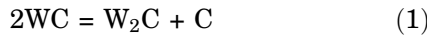
X-ray Diffraction

To determine the phase composition of the cladding layer, the cladding layer was analyzed by x-ray diffraction, and its XRD pattern is shown in Fig. 4. The cladding layer of the S1 sample is mainly composed of γ-(Ni, Cr, Fe), M_7C_3, $M_{23}C_6$, WC, and W_2C, etc. After adding Ta powder, the main phase in the cladding layer was the same as that without Ta powder. The difference is that, after adding Ta powder, a TaC diffraction peak was detected, and the intensity and number of diffraction peaks of the TaC phase increased with increasing Ta powder content. The in situ-synthesized TaC was helpful for improving the microhardness and wear resistance of the cladding layer. However, a part of the C required for in situ synthesis came from the decomposition of WC particles. The formation of many TaC particles means that a large number of WC particles in the molten pool decomposed, which reduces the performance of the cladding layer.
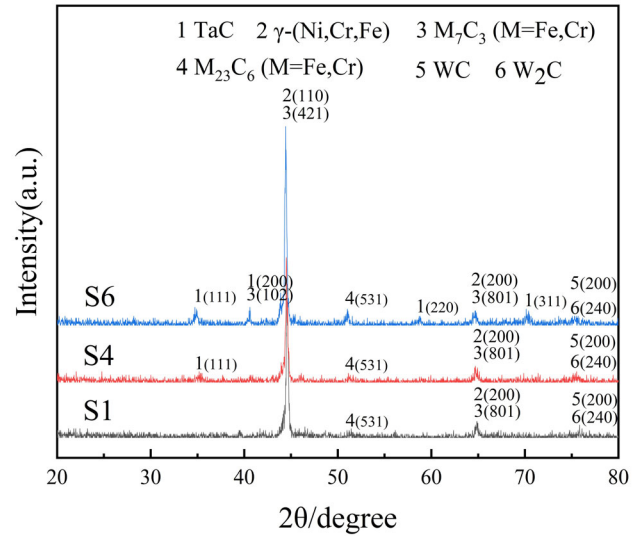

Fig. 4. XRD pattern of the S1, S4, and S6 cladding layers.

Microstructure

Figure 5 shows the microstructure of the top of the cladding layer of the six groups of samples, and Table II shows the EDS analysis results of the top of the cladding layer. C is a light element, and has a strong impact on the test results, so it was not analyzed. Figure 5 shows that the addition of Ta powder had a significant effect on the microstructure of the Ni60A/WC composite coating. When Ta powder was not added, the precipitates at the top of the cladding layer were mostly block or dendritic in structure. According to the EDS results in Table II, the content of W in the highlighted block structure and dendritic structure was significantly higher than that in the surrounding area. Combined with the XRD results, it can be seen that the WC and W_2C hard phases were present. After adding 2 wt.%
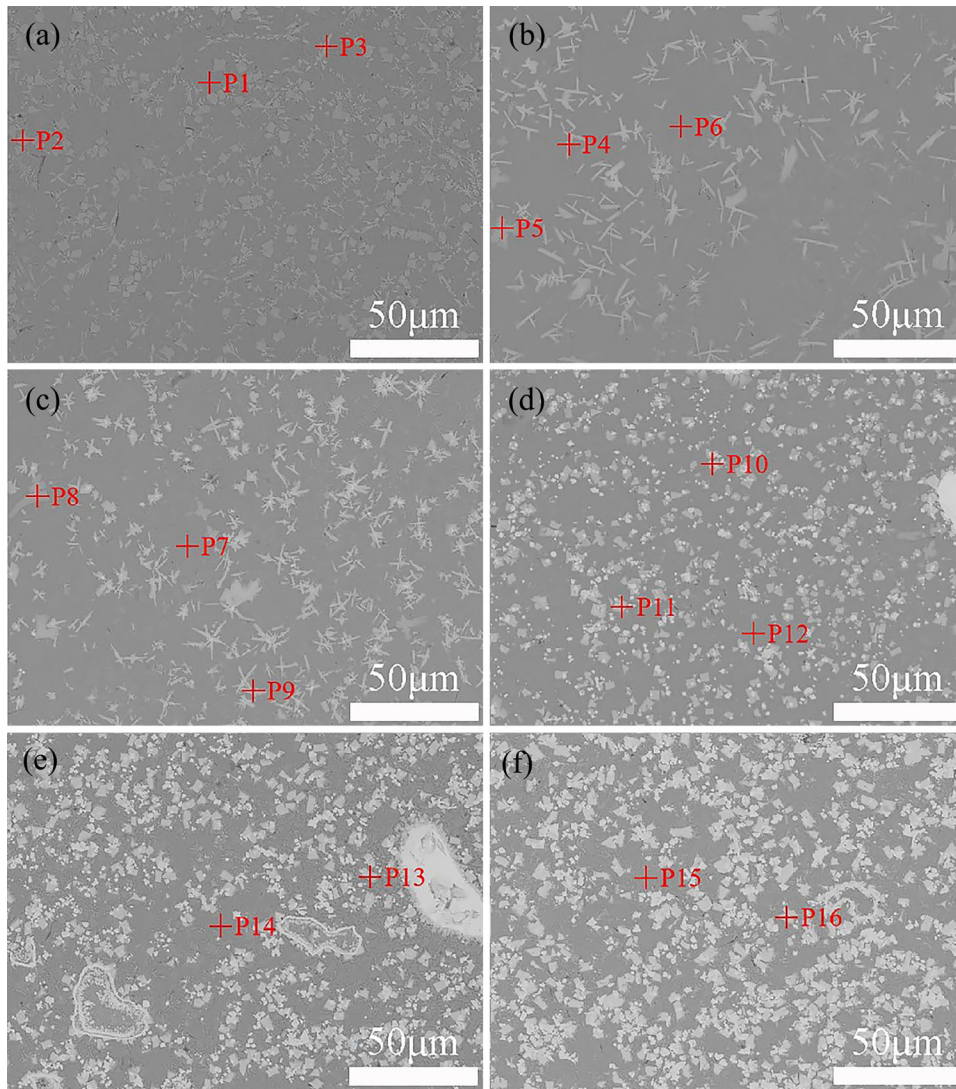
Fig. 5. Microstructure of the top of the cladding layer of six groups of samples: (a) S1, (b) S2, (c) S3, (d) S4, (e) S5, and (f) S6.

of Ta powder, the microstructure of the top of the cladding layer changed substantially, the block structure decreased significantly, and no dendritic structure was found, mostly showing a slender needle-like structure. Since the W-L (8.397 keV) and Ta-L (8.146 keV), and the W-M (1.70 keV) and Ta-M (1.77 keV), characteristic x-ray lines are in close proximity, EDS does not precisely analyze the composition of the coating. Therefore, the high content of Ta may include some tungsten or tungsten carbide particles.[20] From the EDS analysis, it can be found that the needle-like structure was mainly composed of Cr, Ta, and W. Combined with the analysis of the XRD results, it is speculated that the needle-like structure is the carbide of Ta, Cr, and W. After adding 5 wt.% of Ta powder, the slender needle-like structure was further refined, and its number increased significantly. The main reason is that the addition of 5% Ta content accelerates the decomposition of WC, but the

generated TaC has fewer heterogeneous nucleation points, and so the needle-like W_2C is effectively grown. When the content of Ta powder was 10 wt.%, a large amount of TaC precipitates preferentially nucleates heterogeneously, the slender needle-like and rod-like structures disappeared completely, and were replaced with a large number of fine and evenly distributed square and triangular "core–shell" precipitates. With a continuous increase in Ta powder content, the size of the precipitates in the cladding layer also increased, but their shapes showed no obvious change.

To further explore the formation mechanism for "core–shell" precipitates in the cladding layer, the microstructure of "core–shell" precipitates at the top of the cladding layer of the S4 sample was observed by SEM, and the elemental distribution around the structure was analyzed by EDS, and the results are shown in Fig. 6. In the SEM images of the precipitates, it can be seen that the precipitates had a

Table II. EDS results on top of cladding

Point	Atomic concentration %				
	Cr	**Fe**	**Ni**	**Ta**	**W**
P1	11.736	9.407	62.556	–	16.301
P2	36.963	1.263	30.279	–	31.494
P3	8.132	8.215	70.748	–	12.905
P4	25.861	–	18.651	33.242	22.246
P5	13.206	–	53.739	19.960	13.095
P6	9.036	7.702	70.594	12.668	–
P7	9.579	8.473	69.708	12.241	–
P8	20.847	–	44.442	21.833	12.878
P9	36.359	–	16.383	25.909	21.350
P10	28.608	–	22.339	10.462	38.591
P11	27.319	–	21.744	14.977	35.960
P12	7.547	5.273	75.637	11.544	–
P13	12.052	–	20.030	29.691	38.227
P14	9.958	3.878	70.978	15.186	–
P15	14.744	8.015	56.710	20.531	–
P16	10.710	–	23.690	40.165	25.435

polygonal structure, the middle section was bright white, and the surroundings were relatively dark. Based on the theory of backscattered electron imaging, we can see that the contrast of the backscattered electron image of SEM is closely related to the atomic number. Therefore, it is speculated that the atomic number of the middle section was higher, and that the atomic number of the surrounding area was lower. From the elemental distribution diagram, it can be found that the middle part of the precipitate is rich in Ta and C elements. Combined with the XRD analysis, it is speculated that the region was TaC formed in situ in the molten pool. The melting point of TaC is 3880°C. When the molten pool solidifies, it will first nucleate in the liquid phase, providing heterogeneous nucleation points for other free alloy elements in the liquid phase.[21] The outer layer of the precipitate was rich in Cr, which may be due to the strong affinity of Ta for C atoms, due to which Ta reacts more easily with C than with Cr. Therefore, when TaC is formed in situ, the concentration of the surrounding C decreases so that Cr cannot react with C, inhibiting the formation of CrC, Cr_3C_2, Cr_7C_3, and other phases, leading to the accumulation of higher concentrations of Cr around TaC. In addition, the existence of TaC particles reduces the formation-free energy of the Cr-rich phase. When the concentration meets the nucleation conditions, the Cr-rich phase nucleates and grows with TaC particles as heterogeneous nucleation points, which can reduce the cracking sensitivity of the cladding layer.

Microhardness

To reveal the effect of the added Ta powder content on the microhardness of the cladding layer, the microhardness distribution from the top of the cladding layer to the substrate is shown in Fig. 7. and the test diagram is shown in supplementary Fig. S-3. Figure 7 shows that the microhardness of the six groups of samples show a decreasing distribution from the top of the cladding layer to the substrate. The hardness at the top of the cladding layer first increases and then decreases with the addition of Ta. The microhardness of the top of the cladding layer of the S1 sample was 760 HV. After adding an appropriate amount of Ta powder, the microhardness of the top of the cladding layer increased. On the one hand, according to Figs. 4 and 5, after adding Ta powder, uniformly distributed TaC was formed in situ in the molten pool, which can inhibit grain growth, thereby increasing the dispersion and fine grains. On the other hand, from the EDS results at the top of the cladding layer in Table II, it can be seen that there were trace amounts of W and Ta in the nickel-based alloy. Therefore, it is speculated that large atoms, such as W and Ta, are dissolved in the nickel-based alloy, resulting in lattice distortion, increasing the resistance of dislocation movement, and improving the microhardness of the cladding layer. When the content of Ta powder continued to increase, the microhardness of the cladding layer decreased. According to Fig. 3a and b, it can be seen that excess Ta accelerates the dissolution of WC, and, combined with the research conclusions of Ping et al.,[22] it has been found that excess Ta will lead to a substantial increase in the heat capacity of the coating. The increase of laser energy indirectly leads to serious thermal damage and high-hardness loss of pristine WC.[23] In addition, it can be seen in Fig. 7 that, compared with the S1 sample, the microhardness of the S4 sample fluctuated less, and its downward trend was relatively gentle, which indicates that the microstructure of the coating was more uniform.

Wear Resistance

Figure 8 shows the friction coefficient and wear volume of the six groups of samples. In the stable wear stage, the friction coefficient of the cladding layer of the S1 sample was approximately 0.49, and the wear volume was 4.98×10^{-3} mm^3. The friction coefficient and wear volume decreased with increasing Ta powder content. When the content of Ta powder was 10 wt.%, the wear resistance of the S4 cladding layer was better than that of the other samples, its friction coefficient
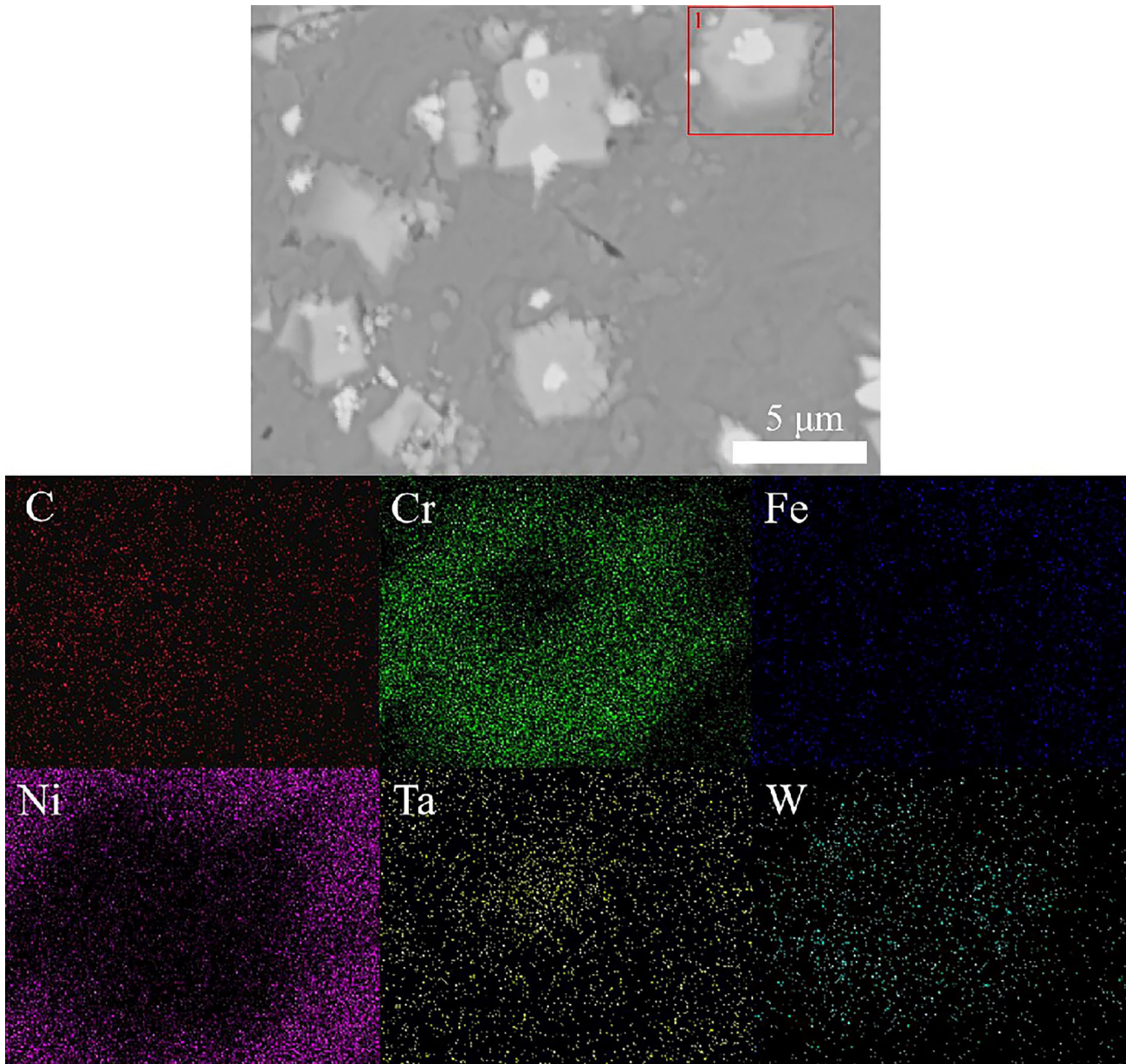
Fig. 6. EDS elemental maps of the S4 top region.

decreased to 0.4, and the wear volume was only 2.73×10^{-3} mm^3. On the one hand, the hardness of the cladding layer was improved by adding an appropriate amount of Ta. On the other hand, the hard phases, such as TaC formed in situ in the cladding layer, played a certain anti-friction role and reduced the wear volume. With a continuous increase in Ta powder content, the friction coefficient and wear volume showed an upward trend. When the content of Ta powder was 20 wt.%, the friction coefficient increased to 0.48, there was a certain fluctuation, and the wear volume increased to 3.94×10^{-3} mm^3. The increase in wear volume

may be related to the decrease in microhardness of the cladding layer, and the fluctuation of the friction coefficient may be because the cladding layer has a variety of dissolved elements, resulting in the improvement of brittleness. It is then easy to produce cracking or microcracks in the friction process, which will be further demonstrated in the follow-up observations.

Figure 9 shows the 3D morphology and outline of the wear track. From Fig. 9a, it can be seen that there were obvious grooves on the wear surface of the S1 sample along the sliding direction of the friction pair. The wear track width was

approximately 0.5 mm, and the wear track depth was approximately 5.3 μm. The surface was severely worn. With increasing Ta powder content, as shown in Fig. 9b, the wear track surface of the S4 sample was relatively smooth, the wear track width decreased to 0.4 mm, the wear track depth decreased to 3.8 μm, and the wear resistance of the cladding layer improved. When the content of Ta powder increased to 20 wt.%, as shown in Fig. 9c, there was an noticeable groove in the middle of the wear track of the S6 sample. The wear track width increased to 0.45 mm, and the wear track depth increased sharply to 4.9 μm, which means that the addition of excess Ta powder will deteriorate the wear resistance of the cladding layer.

To further evaluate the difference in the wear mechanism of coatings with different Ta powder contents, the morphology of the wear track surface was observed by SEM, as shown in Fig. 10. It can be seen from Fig. 10a that there were many clearly visible grooves on the wear track surface of the S1 sample, which indicates that the WC particles in the S1 sample have poor bonding with the nickel-based alloy, and easily fall off during the friction process. These particles remained between the friction pair and the wear surface, acting as abrasive particles. Parallel microgrooves are generated under the relative movement of the friction pair and the wear surface. Therefore, the wear mechanism of the cladding layer of the S1 sample was mainly abrasive wear. After adding a specific amount of Ta powder, as shown in Fig. 10b and c, the number of grooves significantly decreased compared with S1. This may be due to the in situ formation of fine TaC particles in the cladding layer, which effectively reduces the plastic shear effect of the friction pair on the cladding layer. Therefore, the wear mechanism of the cladding layer of the S2 and S3 samples was slight abrasive wear. When the content of Ta powder was 10 wt.%, there was little wear debris on the wear surface, no obvious grooves were found, and the wear surface was relatively smooth, showing good friction characteristics, which was due to the high microhardness of the cladding layer. Therefore, the wear mechanism of the cladding layer of the S4 sample may be in the stage of transformation from abrasive wear to adhesive wear. When the addition content of Ta powder continued to increase, as shown in Fig. 10e and f, there was much wear debris on the wear surface, and there were also some spalling pits on the wear track surface of the S6 sample. This is because the wear surface, in the process of sliding friction, is squeezed by the friction pair and the friction force, which makes the temperature at the contact between the friction pair and the wear surface rise rapidly, resulting in metal adhesion. In the
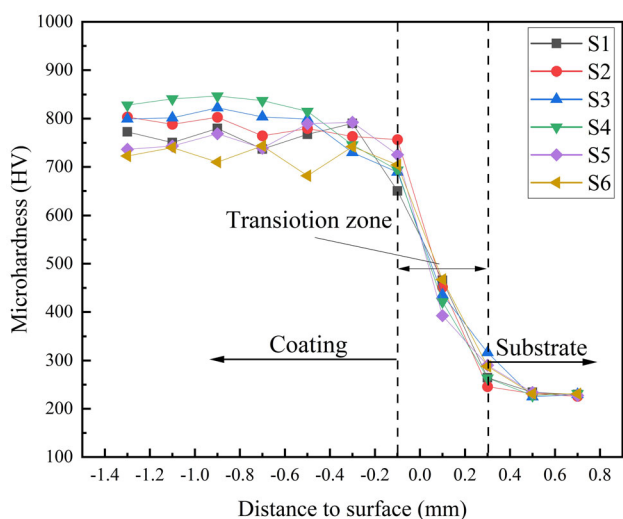

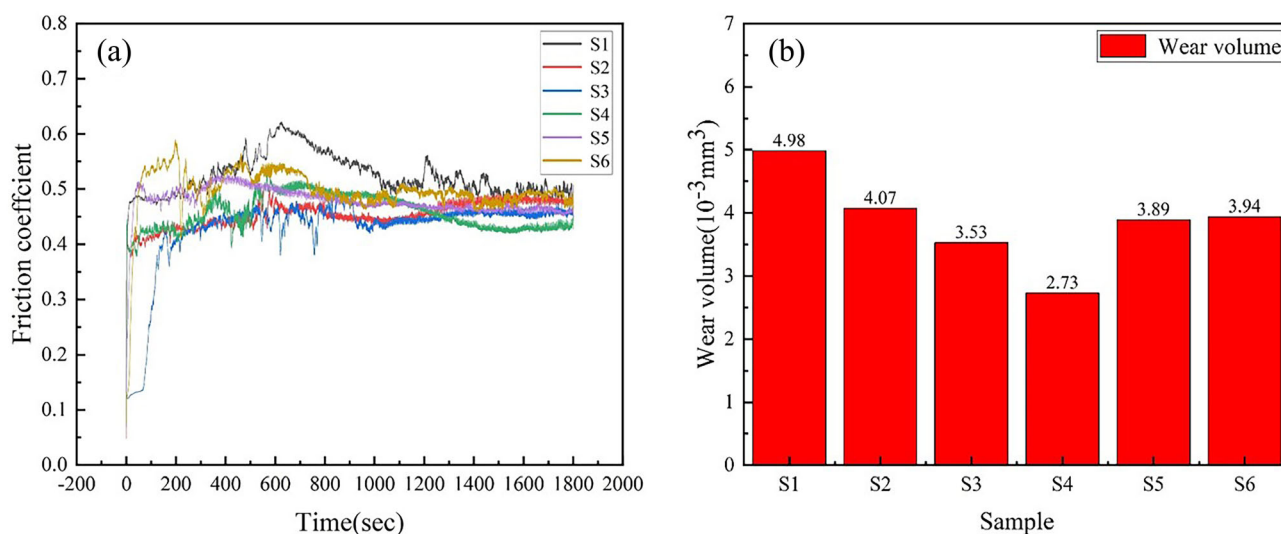Fig. 7. Microhardness curve of the cladding layer.

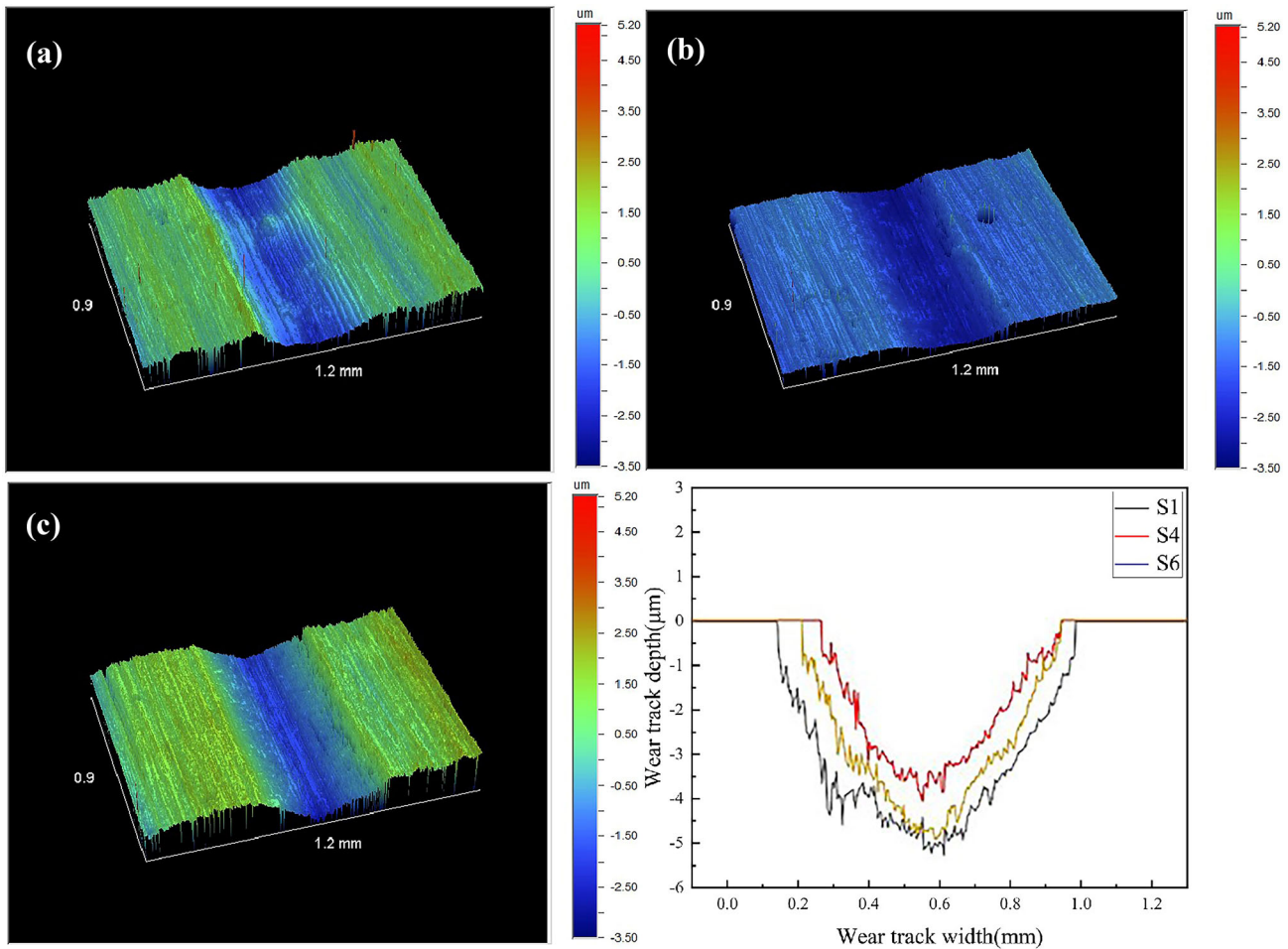Fig. 8. Experimental results of (a) friction coefficient and (b) wear volume.

Fig. 9. 3D morphology: (a) S1, (b) S4, and (c) S6.

subsequent relative sliding, the adhesion was torn and, finally, spalling pits were formed. This means that the wear mechanism of the coating was severe adhesive wear. Therefore, adding an appropriate amount of Ta powder is conducive to improving the wear resistance of the Ni60A/WC composite coating.

CONCLUSION

A Ni60A/WC composite coating with Ta powder was successfully prepared on the surface of 45 steel by laser cladding technology. The effects of different Ta powder contents (0%, 2%, 5%, 10%, 15%, and 20%) on the phase composition, microstructure, microhardness, and friction properties of the Ni60A/WC composite coating were studied. The following conclusions were drawn:

1. After adding Ta powder, the main phases in the cladding layer are TaC, γ-(Ni, Cr, Fe), M_7C_3, $M_{23}C_6$, WC, and W_2C. Compared to the cladding layer without Ta powder, a TaC diffraction peak appears after adding Ta powder, the number of TaC diffraction peaks increases, and the intensity increases with increasing Ta content.

2. After adding an appropriate amount of Ta powder, the dissolution of WC particles is promoted, the morphology of WC hard phase particles tends to be round, and the cracking sensitivity of the cladding layer is reduced. In addition, TaC is formed in situ in the molten pool, which refines the microstructure of the cladding layer and promotes the uniform distribution of the hard phase.

3. With increasing Ta powder content, the microhardness and wear resistance of the composite coating first increases and then decreases. This finding is closely related to the refinement of the microstructure, the uniform distribution of the hard phase, and the dissolution of the WC particles.

4. Among the six groups of samples, the microhardness of the S4 coating with 10 wt.% Ta powder is the highest, reaching 840 HV, which is 10.5% higher than that of the S1 coating without Ta powder. In addition, the fine TaC particles synthesized in situ can reduce the plastic shear effect of the friction pair on the cladding layer, which also improves the friction properties of the coating. Among the coatings, the S4 coating has the best friction performance,
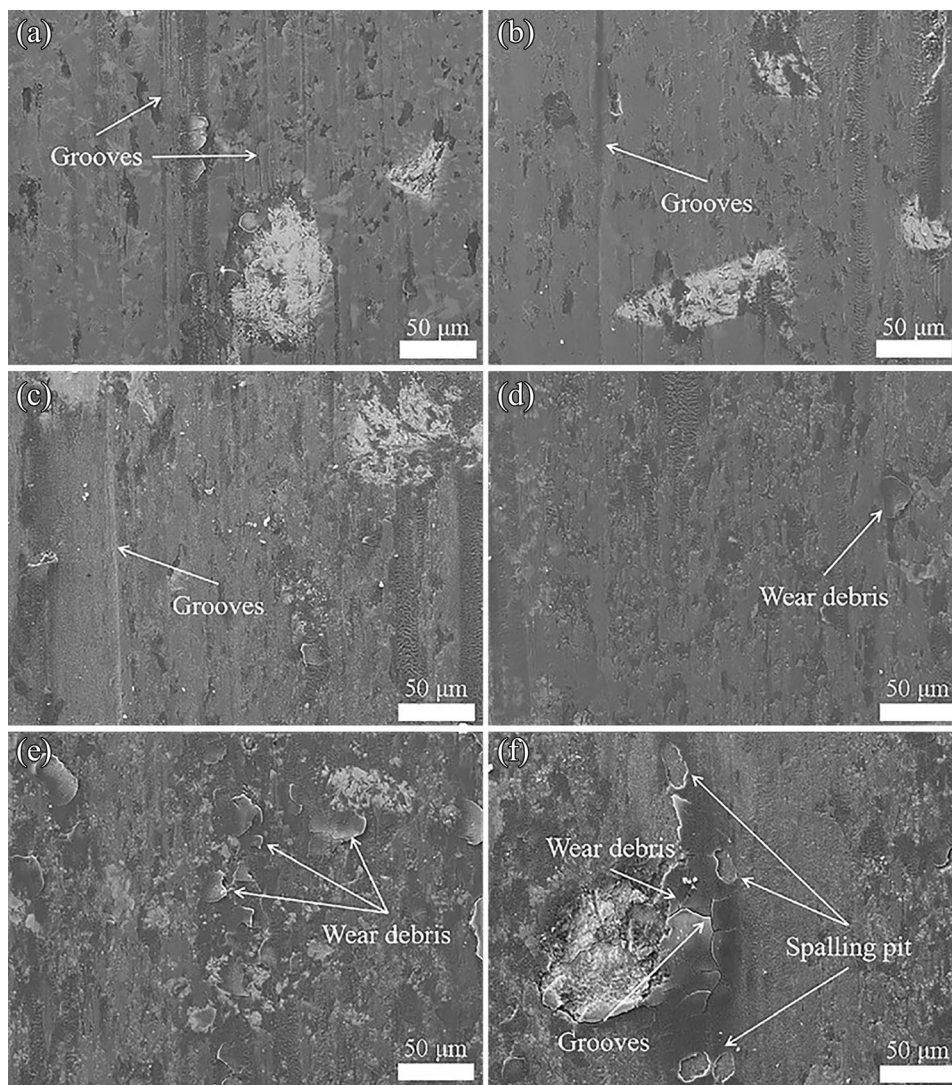
Fig. 10. SEM images of wear tracks: (a) S1, (b) S2, (c) S3, (d) S4, (e) S5, and (f) S6.

with the friction coefficient and wear volume of 0.4 and 2.73×10^{-3} mm^3, respectively.

DATA AVAILABILITY

The data that support the findings in this paper available from the corresponding authors upon reasonable request.

CONFLICT OF INTEREST

The authors declare that they have no known competing financial interests or personal relationships that could have appeared to influence the work reported in this paper.

SUPPLEMENTARY INFORMATION

The online version contains supplementary material available at https://doi.org/10.1007/s11837-022-05502-x.

REFERENCES

1. B. Haldar and P. Saha, *Proc. Manuf.* 20, 446–451. https://doi.org/10.1016/j.promfg.2018.02.065 (2018).

2. F. Wang, C. Li, S. Sun, M. Zeng, C. Liu, Q. Lu, and Y. Wang, *Jom* 72, 4060–4068. https://doi.org/10.1007/s11837-020-04322-1 (2020).

3. W. Li, X. Yang, J. Xiao, and Q. Hou, *Ceram. Int.* 47, 28754–28763. https://doi.org/10.1016/j.ceramint.2021.07.035 (2021).

4. A. Gowtham, G. Chaitanya, J.K. Katiyar, A. Chandak, and T.V.K. Gupta, *Mater. Today: Proc.* 27, 1984–1989. https://doi.org/10.1016/j.matpr.2019.09.044 (2020).

5. C. Schulz, T. Schläfer, J. Plowman, and C. Hall, *Jom* 72, 4624–4631. https://doi.org/10.1007/s11837-020-04390-3 (2020).

6. H. Wang, Y. Sun, Y. Qiao, and X. Du, *Optics Laser Technol.* https://doi.org/10.1016/j.optlastec.2021.107209 (2021).

7. J. Skamat, O. Černašėjus, Ž Čepukė, and N. Višniakov, *Surf. Coat. Technol.* 374, 1091–1099. https://doi.org/10.1016/j.surfcoat.2019.06.080 (2019).

8. Y. Peng, W. Zhang, T. Li, M. Zhang, B. Liu, Y. Liu, L. Wang, and S. Hu, *Surf. Coat. Technol.* https://doi.org/10.1016/j.surfcoat.2019.125326 (2020).

9. I. Hulka, D. Utu, V.A. Serban, P. Negrea, F. Lukáč, and T. Chráska, *Appl. Surf. Sci.* https://doi.org/10.1016/j.apsusc.2019.144349 (2020).

10. L. Liu, W. Wang, X. Zhang, X. Li, Y. Tian, and X. Zhao, *Mater. Sci. Eng. A.* https://doi.org/10.1016/j.msea.2021.141238 (2021).

11. Y.H. Lv, J. Li, Y.F. Tao, and L.F. Hu, *J. Alloy. Compd.* 679, 202–212. https://doi.org/10.1016/j.jallcom.2016.04.037 (2016).

12. J. Peng, H. Dong, M. Hojamberdiev, D. Yi, Y. Yang, H. Bao, H. Li, H. Li, D. Mao, and L. Meng, *J. Alloy. Compd.* 726, 896–905. https://doi.org/10.1016/j.jallcom.2017.08.050 (2017).

13. D. Hu, Y. Liu, H. Chen, J. Liu, M. Wang, and L. Deng, *Opt. Laser Technol.* https://doi.org/10.1016/j.optlastec.2021.107210 (2021).

14. Q.L. Deng, W. Fu, and H.Y. Fang, *Mater. Sci. Forum* 893, 323–329. https://doi.org/10.4028/www.scientific.net/MSF.893.323 (2017).

15. Q. Xiao, W.L. Sun, K.X. Yang, X.F. Xing, Z.H. Chen, H.N. Zhou, and J. Lu, *Surf. Coat. Technol.* https://doi.org/10.1016/j.surfcoat.2021.127341 (2021).

16. T. Yamaguchi and H. Hagino, *Opt. Laser Technol.* https://doi.org/10.1016/j.optlastec.2021.106922 (2021).

17. X. He, R.G. Song, and D.J. Kong, *Opt. Laser Technol.* 112, 339–348. https://doi.org/10.1016/j.optlastec.2018.11.037 (2019).

18. M.A. Islam, J. Jiang, and Y. Xie, *Wear.* https://doi.org/10.1016/j.wear.2021.203820 (2021).

19. N. Zhao, Y. Xu, L. Zhong, Y. Yan, K. Song, L. Shen, and V.E. Ovcharenko, *Ceram. Int.* 41, 12950–12957. https://doi.org/10.1016/j.ceramint.2015.06.138 (2015).

20. Y. Yaowei, F. Wei, Z. Xiang, D. Qilin, and Y. Jianguo, *Rare Metal Mater. Eng.* 46, 3176–3181. https://doi.org/10.1016/s1875-5372(18)30024-9 (2017).

21. Y.H. Lv, J. Li, Y.F. Tao, and L.F. Hu, *Appl. Surf. Sci.* 402, 478–494. https://doi.org/10.1016/j.apsusc.2017.01.118 (2017).

22. P. Cai, Q. He, L. Yang, Z. Huang, X. Liu, J. Yin, and Y. Huang, *Ceram. Int.* 45, 9799–9806. https://doi.org/10.1016/j.ceramint.2019.02.017 (2019).

23. X. Wang, S. Zhou, X. Dai, J. Lei, J. Guo, Z. Gu, and T. Wang, *Int. J. Refract Metal Hard Mater.* 64, 234–241. https://doi.org/10.1016/j.ijrmhm.2016.11.001 (2017).